Femtosecond laser textured porous nanowire structured glass for enhanced thermal imaging

Tingni Wu (吴婷妮)[1], Zhipeng Wu (吴志鹏)[1], Yuchun He (何玉春)[1], Zhuo Zhu (朱 卓)[1], Lingxiao Wang (王凌霄)[1], and Kai Yin (银 恺)[1,2*]

[1] Hunan Key Laboratory of Nanophotonics and Devices, School of Physics and Electronics, Central South University, Changsha 410083, China

[2] State Key Laboratory of High Performance and Complex Manufacturing, College of Mechanical and Electrical Engineering, Central South University, Changsha 410083, China

*Corresponding author: kaiyin@csu.edu.cn

Infrared (IR) thermal imaging has aroused great interest due to its wide application in medical, scientific, and military fields. Most reported approaches for regulating thermal radiation are aimed to realize IR camouflage and are not applicable to enhance thermal imaging. Here, we introduce a simple and effective method to process porous glass by femtosecond laser scanning, where distributed nanocavities and nanowires were produced, which caused improvement of the treated glass emissivity. The as-prepared sample possessed better IR thermal radiation performance but lower transmittance to visible light. We also demonstrated its applicability by placing it in different backgrounds, where the IR image temperature of laser-treated glass was closer to the actual environment, and this strategy may provide a new vision for enhanced thermal imaging.

Keywords: femtosecond laser; thermal radiation; texture; micro/nanostructures; glass.
DOI: 10.3788/COL202220.033801

1. Introduction

Any object with a temperature higher than absolute zero will emit thermal radiation as stated in Planck's law[1]. According to the Stefan–Boltzmann law, the total thermal energy radiated from the surface of an object is proportional to the emissivity ε and the fourth power of the temperature. Thus, the infrared (IR) imaging can be controlled by either regulating the emissivity or changing the surface temperature. In nature, many organisms achieve better survival by adjusting their own IR radiation[2–4]. Inspired by natural creatures, imitate biological regulation of surface heat radiation to achieve personal thermal management[5,6], IR camouflage[7,8], IR radiation cooling[9,10], and other functions[11–13] has received widespread attention.

IR imaging can be controlled by either regulating the emissivity or changing surface temperature, which is based on Stefan's law. Extensive technologies on adjusting the thermal radiation have been reported so far, such as chemical coating, ultraviolet lithography[14], and other methods[15,16]. Zhu et al. completed the high-temperature IR camouflage, which is based on the combination of the SiO_2 aerogel and the Ge/ZnS wavelength-selective emitter[8]; Kirchhoff's law, which exhibits the absorptivity equal to emissivity during thermo-dynamic equilibrium, played a vital role in the design of the micro/nanostructures to tailor the thermal radiation properties. Based on this

consideration, Qu et al. designed the two kinds of spatially and spectrally resolved narrowband absorbers supported by 2D grating nanostructures and gold upon metallic film[17]. Qi et al. reported a kind of photonic crystals (PCs) with very low IR emissivity to meet the target of IR stealth, acquired by constructing a one-dimensional PC (1DPC) structure of $Hs(Ge/ZnS)^3Ge$[18]. Nevertheless, these studies are almost reporting on methods of decreasing IR radiation, and there were few reports about improving IR radiation. Moreover, the above-mentioned fabrication procedures are complicated and challenging to operate. As a result, it is necessary to explore a simple and rapid way to increase IR radiation.

Herein, the femtosecond laser direct writing technology was applied to process micro-nano structured glass, the absorption of visible light and emissivity of IR light rise due to the production of the micro/nanostructures, and the size of nanocavities is about 200–500 nm. The laser-ablated (LT) glass exhibits lower transmittance of 16%–51%, accounting for the enhancement of scattering sunlight and higher absorption of 8%–16.4% at the visible wavelength than the untreated (UT) glass. In the IR wavelength range, it can also be observed that the emissivity of the LT glass is significantly increased, which leads to an improvement in the outward radiation heat. We experimentally demonstrate that higher IR image temperature appeared after processing, and

the IR image of the LT glass is always closer to the actual environmental temperature than the UT sample wherever they were placed, which proved that the processed sample has better IR thermal imaging.

2. Experimental Section

2.1. Preparation of porous structure

Femtosecond lasers can be used to fabricate micro/nanostructures, changing the properties of materials and opening up new applications[19–29]. In this experiment, we employed a high-repetition commercial femtosecond laser system (PHAROS, LIGHT CONVERSION, Lithuania) with the frequency, central wavelength, and pulse width of 75 kHz, 1030 nm, and 250 fs, respectively. The laser beam was guided onto the substrate surface through a two-mirror galvanometric scanner (intelliSCAN III 14, SCANLAB, Germany) with an FTheta lens ($f = 100$ mm). Laser power, scanning line speed, and scanning line spacing were controlled as 6 W, 0.2 m/s, and 10 μm, respectively. A 20 mm × 20 mm glass (purchased from Guluo Quartz Glass Company, Luoyang) of 1 mm thickness is fixed to a processing stage. The rough surface of the glass was then fabricated by the line-by-line femtosecond laser scanning process.

2.2. Characterization

The three-dimensional (3D) morphology and cross-section height were characterized by laser confocal microscopy (LCM, Axio LSM700, Zeiss, Germany). The micro/nanostructures of the treated surface were investigated using scanning electron microscopy (SEM, MIRA3 LMU, TESCAN, Czech Republic), and the analysis of elemental composition and elemental maps was carried out by energy-dispersive X-ray spectroscopy (EDS, TESCAN, Czech Republic). Absorption and transmittance spectra were recorded using an ultraviolet-visible (UV-vis) spectrophotometer (UV-2600, Japan) with an integrating sphere. The IR emissivity and reflectance were acquired by a Fourier transform IR spectrometer (Nicolet, NEXUS 670). The temperature distribution was obtained by an IR camera (Ti450, Fluke, USA).

3. Results and Discussion

Figure 1(a) shows the schematic illustration of the process of the femtosecond laser ablating glass and the optical principle of the UT and LT glass. The optical performance of these two samples in the visible and IR wavelength ranges has depicted an as-prepared sample with a higher light reflectance, IR emissivity, and lower transmittance. The surface of the sample after laser ablation has changed from smooth to rough, and many randomly distributed nanocavities and nanowires were produced. SEM images further reveal that [Figs. 2(a)–2(c)] at a finer scale. On account of the generation of these micro/nanostructures, light is irradiated on the object's surface, and more refraction and scattering will occur. Similarly, the 3D and cross-sectional
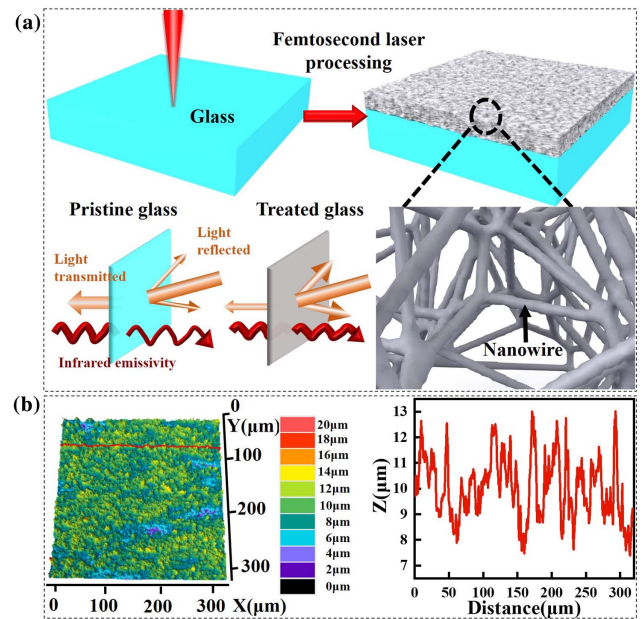

Fig. 1. (a) Schematic diagram of the laser ablation on one glass side and the optical principle before and after processing (lower left part). (b) Topography in 3D and section height map of laser-treated glass.
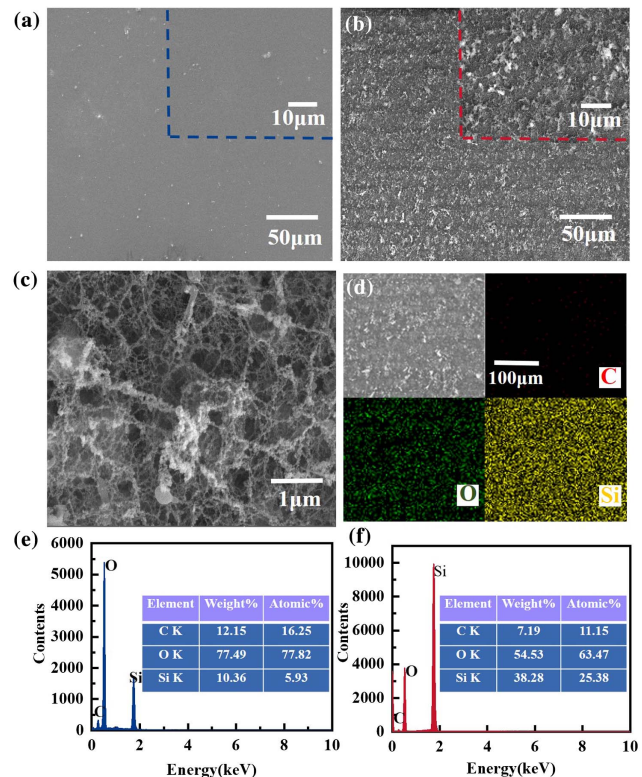

Fig. 2. (a)–(c) SEM images of the (a) UT and (b), (c) LT glass surfaces. Insets: high-resolution SEM images of the respective surfaces. (d) Element maps and (e), (f) EDS spectra of the (e) UT and (f) LT glass surfaces.

profiles were tested by LCM to evaluate the influence of femto-second laser ablation [Fig. 1(b)], and it discovered that the surface roughness was relatively uniform.

Figures 2(a)–2(c) show the SEM topography of the UT and LT surface. It is evident that the surface of the LT glass has become much rougher than the UT sample [Fig. 2(a)], and the surface roughness after machining is homogeneous [Fig. 2(b)]. After further magnification, it can be found that there are many nano-wires and nanocavities uniformly and randomly distributed on the surface. Nanowires in some regions are sintered together, and this may be due to the higher temperature during the pro-cedure. The diameters of the nanocavities are 200 to 500 nm, which scatter visible light strongly and make the LT glass opaque to human eyes. The sizes of the holes are also much smaller than the IR wavelength, so it is beneficial to enhance IR radia-tion[8]. The characterized morphology and roughness are overall very consistent with the LCM images, further proving that the fabricated micro/nanostructures by our strategy are uniform. Femtosecond laser ablation of glass in the air may produce chemical reactions and lead to changes in the content of chemi-cal elements[30], so EDS was used to compare and analyze the elements on the surface of the LT and UT. EDS mapping presents the elements being evenly distributed after processing.

The rough surfaces constructed by diverse micro/nanostructures are totally opaque because of the extensive light scattering effect. When the LT sample is placed on a paper with patterns, the fuzzy patterns behind the sample can be observed [Fig. 3(a)]. On the con-trary, the pattern is obviously exhibited when the sample is placed under the UT glass. Therefore, to compare the influence of the

LT sample surface more accurately, we measured the absorptivity and transmittance of the samples, respectively [Fig. 3(a)]. In the wavelength range of 220–1400 nm, the transmittance of the UT glass is higher than that of the LT glass from 12% to 50%. The absorption value of UT samples is about 10% lower than that of the LT glass, which is calculated based on the relation $\alpha + \rho + \tau = 1$ (where α is absorption, τ is transmission, and ρ is reflection). Moreover, similar phenomena can be observed at IR wavelengths, where the emissivity increases are attributed to the existence of the special structures, which leads to the LT glass being able to absorb a large amount of light energy [Fig. 3(b)]. However, the trend of reflectance appears inverse, and the spectral reflectance of the LT glass is consistently lower than that of the UT sample at the wavelength of 2.5–25 µm.

IR images were recorded to show the capacity of the LT sam-ple to achieve the improvement of thermal imaging at different conditions. The surface of the heater was partly covered with two pieces of insulating cotton, which were used to prevent the heater and the sample from contacting directly [Fig. 4(a)]. When the constant temperature was set at 150°C, the real-time thermal imaging was recorded by the IR camera every 30 s, and the time when the sample was put on the heater was considered as the initial time [Fig. 4(b)]. As shown in Fig. 4(c), for the UT and LT areas, the temperature rose quickly in the first 60 s and then stabilized after about 110 s. After stabilization, the temper-ature of the UT and LT areas was recorded as about 81.2°C and 72.6°C, respectively. During the whole procedure, the tempera-ture of the LT glass surface is always higher than that of the UT surface, which is attributed to the higher emissivity of the LT region. The UT and the LT glasses, with entirely the same size of 2 cm × 2 cm, were placed on the hand, respectively [Fig. 4(d)]. The area covered with the LT glass becomes nearly invisible under the IR camera, as its surface temperature is too
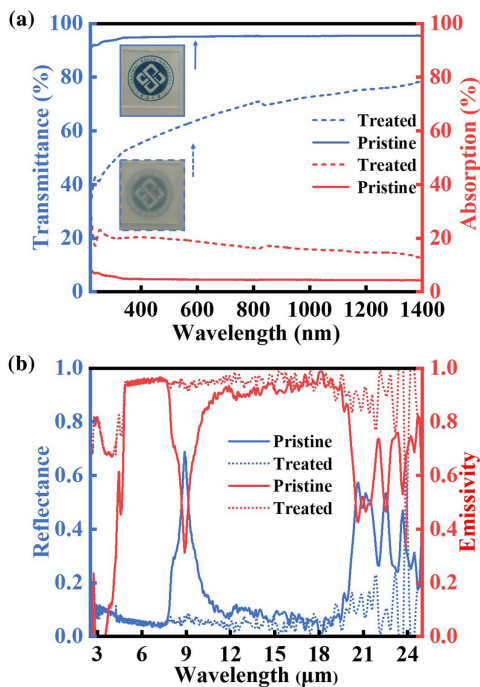
Fig. 3. (a) Absorption, transmittance and (b) emissivity, reflectance over dif-ferent wavelength ranges. Insets in (a) show the optical images of samples before and after laser treatment.
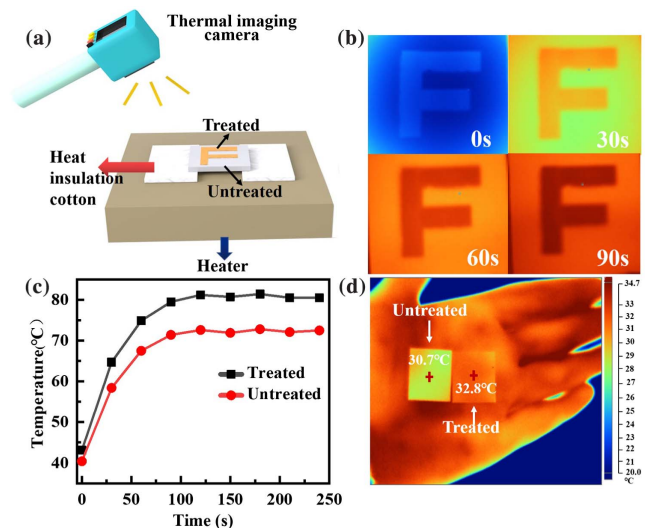
Fig. 4. (a) IR thermal imaging experimental device. (b) IR thermal images. (c) The surface temperature of LT and UT changes with time in the corre-sponding experiment. (d) IR thermal images of LT and UT glasses when they are placed on the hand.

close to the hand, which is caused by the micro/nanostructures being induced during the processing. The temperature of the UT sample is lower by about 2° than the other. All of the data shown above illustrate that the glass ablated by the femtosecond laser can enhance IR imaging.

4. Conclusion

In summary, one-sided rough micro/nanostructures glass was fabricated through a one-step femtosecond laser direct writing technology. Due to the micro/nanostructures such as nanocavities (about 200–500 nm in diameter) and nanowires appearing on the surface, this leads to a lot of light energy confined to micro/nanostructures. Thus, the absorption and emissivity in the wavelength range of visible light and IR light rise. When the LT sample was directly placed on the object, the IR thermal image of the LT glass was more accurate than that of the UT sample. This work provides a new way to enhance thermal imaging.

Acknowledgement

References

1. D. G. Baranov, Y. Xiao, I. A. Nechepurenko, A. Krasnok, A. Alu, and M. A. Kats, "Nanophotonic engineering of far-field thermal emitters," Nat. Mater. **18**, 920 (2019).
2. E. O. Gracheva, J. F. Cordero-Morales, J. A. Gonzalez-Carcacia, N. T. Ingolia, C. Manno, C. I. Aranguren, J. S. Weissman, and D. Julius, "Ganglion-specific splicing of TRPV1 underlies infrared sensation in vampire bats," Nature **476**, 88 (2011).
3. E. O. Gracheva, N. T. Ingolia, Y. M. Kelly, J. F. Cordero-Morales, G. Hollopeter, A. T. Chesler, E. E. Sanchez, J. C. Perez, J. S. Weissman, and D. Julius, "Molecular basis of infrared detection by snakes," Nature **464**, 1006 (2010).
4. N. N. Shi, C. Tsai, F. Camino, G. D. Bernard, N. Yu, and R. Wehner, "Keeping cool: enhanced optical reflection and radiative heat dissipation in Saharan silver ants," Science **349**, 298 (2015).
5. Y. Guo, K. Li, C. Hou, Y. Li, Q. Zhang, and H. Wang, "Fluoroalkylsilane-modified textile-based personal energy management device for multifunctional wearable applications," ACS Appl. Mater. Interfaces **8**, 4676 (2016).
6. P. Hsu, A. X. Song, P. B. Catrysse, C. Liu, Y. Peng, J. Xie, S. Fan, and Y. Cui, "Radiative human body cooling by nanoporous polyethylene textile," Science **353**, 1019 (2016).
7. X. Xie, M. Pu, Y. Huang, X. Ma, X. Li, Y. Guo, and X. Luo, "Heat resisting metallic meta-skin for simultaneous microwave broadband scattering and infrared invisibility based on catenary optical field," Adv. Mater. Technol. **4**, 1800612 (2019).
8. H. Zhu, Q. Li, C. Zheng, Y. Hong, Z. Xu, H. Wang, W. Shen, S. Kaur, P. Ghosh, and M. Qiu, "High-temperature infrared camouflage with efficient thermal management," Light Sci. Appl. **9**, 60 (2020).
9. C. Zou, G. Ren, M. M. Hossain, S. Nirantar, W. Withayachumnankul, T. Ahmed, M. Bhaskaran, S. Sriram, M. Gu, and C. Fumeaux, "Metal-loaded dielectric resonator metasurfaces for radiative cooling," Adv. Opt. Mater. **5**, 1700460 (2017).
10. S. Atiganyanun, J. B. Plumley, S. J. Han, K. Hsu, J. Cytrynbaum, T. L. Peng, S. M. Han, and S. E. Han, "Effective radiative cooling by paint-format microsphere-based photonic random media," ACS Photonics **5**, 1181 (2018).
11. H. K. Raut, V. A. Ganesh, A. S. Nair, and S. Ramakrishna, "Anti-reflective coatings: a critical, in-depth review," Energy Environ. Sci. **4**, 3779 (2011).
12. D. G. Stavenga, S. Foletti, G. Palasantzas, and K. Arikawa, "Light on the moth-eye corneal nipple array of butterflies," Proc. R. Soc. B **273**, 661 (2006).
13. J. Zhu, Z. Yu, G. F. Burkhard, C. Hsu, S. T. Connor, Y. Xu, Q. Wang, M. McGehee, S. Fan, and Y. Cui, "Optical absorption enhancement in amorphous silicon nanowire and nanocone arrays," Nano Lett. **9**, 279 (2009).
14. Z. Guo, X. Liu, C. Li, J. Li, H. Cai, M. Fu, D. He, and Y. Wang, "Near-perfect broadband metamaterial absorbers of truncated nanocones using colloidal lithography," Opt. Mater. **119**, 111352 (2021).
15. J. Park, J. Kang, X. Liu, Scott J. Maddox, K. Tang, P. C. McIntyre, S. R. Bank, and M. L. Brongersma, "Dynamic thermal emission control with InAs-based plasmonic metasurfaces," Sci. Adv. **4**, eaat3163 (2018).
16. A. Sakurai, K. Yada, T. Simomura, S. Ju, M. Kashiwagi, H. Okada, T. Nagao, K. Tsuda, and J. Shiomi, "Ultranarrow-band wavelength-selective thermal emission with aperiodic multilayered metamaterials designed by Bayesian optimization," ACS Cent. Sci. **5**, 319 (2019).
17. Y. Qu, Q. Li, H. Gong, K. Du, S. Bai, D. Zhao, H. Ye, and M. Qiu, "Spatially and spectrally resolved narrowband optical absorber based on 2D grating nanostructures on metallic films," Adv. Opt. Mater. **4**, 480 (2016).
18. D. Qi, X. Wang, Y. Cheng, R. Gong, and B. Li, "Design and characterization of one-dimensional photonic crystals based on ZnS/Ge for infrared-visible compatible stealth applications," Opt. Mater. **62**, 52 (2016).
19. K. Yin, D. Chu, X. Dong, C. Wang, J. Duan, and J. He, "Femtosecond laser induced robust periodic nanoripple structured mesh for highly efficient oil–water separation," Nanoscale. **9**, 14229 (2017).
20. D. Wu, J. Wang, S. Wu, Q. Chen, S. Zhao, H. Zhang, H. Sun, and L. Jiang, "Three-level biomimetic rice-leaf surfaces with controllable anisotropic sliding," Adv. Funct. Mater. **21**, 2927 (2011).
21. J. Wu, J. He, K. Yin, Z. Zhu, S. Xiao, Z. Wu, and J. Duan, "Robust hierarchical porous PTFE film fabricated via femtosecond laser for self-cleaning passive cooling," Nano Lett. **21**, 4209 (2021).
22. J. Wu, K. Yin, M. Li, Z. Wu, S. Xiao, H. Wang, J. Duan, and J. He, "Under-oil self-driven and directional transport of water on a femtosecond laser-processed superhydrophilic geometry-gradient structure," Nanoscale **12**, 4077 (2020).
23. F. Zhang, C. Wang, K. Yin, X. Dong, Y. Song, Y. Tian, and J. Duan, "Investigation on optical and photoluminescence properties of organic semiconductor Al-Alq3 thin films for organic light-emitting diodes application," Chin. Opt. Lett. **15**, 111602 (2017).
24. K. Yin, Z. Wu, J. Wu, Z. Zhu, F. Zhang, and J. Duan, "Solar-driven thermal-wind synergistic effect on laser-textured superhydrophilic copper foam architectures for ultrahigh efficient vapor generation," Appl. Phys. Lett. **118**, 211905 (2021).
25. D. Chu, K. Yin, X. Dong, Z. Luo, and Y. Song, "Ablation enhancement by defocused irradiation assisted femtosecond laser fabrication of stainless alloy," Chin. Opt. Lett. **16**, 011401 (2018).
26. A. Das and M. Shukla, "Multifunctional hopeite nanocoating on Ti64 substrates by pulsed laser deposition and radio frequency magnetron sputtering for orthopedic implant applications: a comparative study," J. Cent. South Univ. **27**, 2198 (2020).
27. Z. Si, X. Shen, J. Zhu, L. Lin, L. Bai, and J. Liu, "All-reflective self-referenced spectral interferometry for single-shot measurement of few-cycle femtosecond pulses in a broadband spectral range," Chin. Opt. Lett. **18**, 021202 (2020).
28. D. Zhou, X. Zhang, Q. Lu, Q. Liang, and Y. Liu, "Time-resolved study of the lasing emission from high vibrational levels of N^{2+} pumped with circularly polarized femtosecond pulses," Chin. Opt. Lett. **18**, 023201 (2020).
29. Q. Lin, L. Yan, Y. Song, X. Jia, X. Feng, L. Hou, and J. Bai, "Switchable single- and dual-wavelength femtosecond mode-locked Er-doped fiber laser based on carboxyl-functionalized graphene oxide saturable absorber," Chin. Opt. Lett. **19**, 111405 (2021).
30. J. Yang, F. Luo, T. Kao, X. Li, G. Ho, J. Teng, X. Luo, and M. Hong, "Design and fabrication of broadband ultralow reflectivity black Si surfaces by laser micro/nanoprocessing," Light Sci. Appl. **3**, e185 (2014).